ACS NANO
Cite This: ACS Nano XXXX, XXX, XXX–XXX
www.acsnano.org

ARTICLE

Enhanced Transdermal Drug Delivery by Transfersome-Embedded Oligopeptide Hydrogel for Topical Chemotherapy of Melanoma

Tianyue Jiang,[†] Tong Wang,[†] Teng Li,[‡] Yudi Ma,[†] Shiyang Shen,[‡] Bingfang He,*[,†] and Ran Mo*[,‡]

[†]School of Pharmaceutical Sciences, Nanjing Tech University, Nanjing 211816, China

[‡]State Key Laboratory of Natural Medicines, Jiangsu Key Laboratory of Drug Discovery for Metabolic Diseases, Center of Advanced Pharmaceuticals and Biomaterials, China Pharmaceutical University, Nanjing 210009, China

Supporting Information

ABSTRACT: **Topical administration of anticancer drugs provides a potential chemotherapeutic modality with high patient compliance for cutaneous melanoma. However, the drug delivery efficiency is highly limited by physiological barriers from the skin to the tumor, which cannot acquire desired therapeutic efficacy. Herein, we propose a paintable oligopeptide hydrogel containing paclitaxel (PTX)-encapsulated cell-penetrating-peptide (CPP)-modified transfersomes (PTX-CTs) to enhance transdermal PTX delivery for topical melanoma treatment. After being plastered on the skin above the melanoma tumor, the PTX-CTs-embedded hydrogel (PTX-CTs/Gel) as a patch provided prolonged retention capacity of the PTX-CTs on the skin. The PTX-CTs with superior deformability could efficiently squeeze through the channels in the stratum coreum, and the surfactant components improved the fluidity of the lipid molecules in the stratum corneum to further enhance the skin permeation. Moreover, the CPP modification rendered the PTX-CT-enhanced penetration in the skin and tumor stroma as well as efficient transportation in the tumor cells. The PTX-CTs were shown to effectively slow the tumor growth in combination with the systemic chemotherapy using Taxol, the commercial PTX formulation on the xenograft B10F16 melanoma mouse model.**

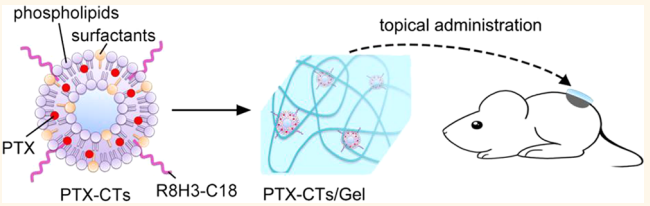

KEYWORDS: *transdermal drug delivery, transfersome, cell-penetrating peptide, oligopeptide hydrogel, melanoma*

Topical drug administration through the skin, ophthalmic, and rectal routes has great potential for treatment of many diseases.[1−3] As the first line of defense in human body, the skin is mainly responsible for resisting pathogen invasion and preventing water loss. The therapeutic benefits of transdermal drug delivery[4,5] have been recognized for many years in comparison with those of other routes of drug delivery, such as convenient self-administration, suitable long-term treatment, avoidance of the first-pass effect, and improved patient compliance. For skin disease, topical application is more effective with high therapeutic concentration and minimized systemic toxicity, which aims to deliver drugs to the skin for local therapy or across the skin for systemic treatment. However, delivery of drugs across the skin barrier is highly challenging. Stratum corneum, the outermost layer of the skin, is the most significant barrier to be overcome for transdermal drug delivery,[6] which serves as a brick-and-mortar system consisting of layers of flattened dead keratinocytes surrounded by a lipid matrix.

Mechanical devices have been used to improve the transdermal efficiency of drugs by physical-enhancement techniques such as electroporation,[7] iontophoresis,[8] magnetophoresis,[9] sonophoresis,[10] and microneedle.[11−13] Alternatively, nanoparticle-based drug delivery systems have been increasingly exploited for transdermal drug delivery,[14,15] such as liposomes,[16] nanoemulsions,[17] dendritic nanocarriers,[18] and inorganic nanosystems.[19,20] Small nanoparticles are more able to penetrate the skin than the larger ones, in general. Gold nanoparticles with a size of 22 nm presented superior penetration ability across the stratum corneum than those with sizes of 105 and 186 nm.[21] Silica nanoparticles larger than 75 nm in size could not penetrate the skin.[22] Transfersomes composed of phospholipids and surfactants hold great potential to enhance the skin permeation efficiency of biomedical molecules, in particular.[23,24] Like liposomes, the

Received: May 20, 2018
Accepted: August 29, 2018

DOI: 10.1021/acsnano.8b03800
ACS Nano XXXX, XXX, XXX–XXX

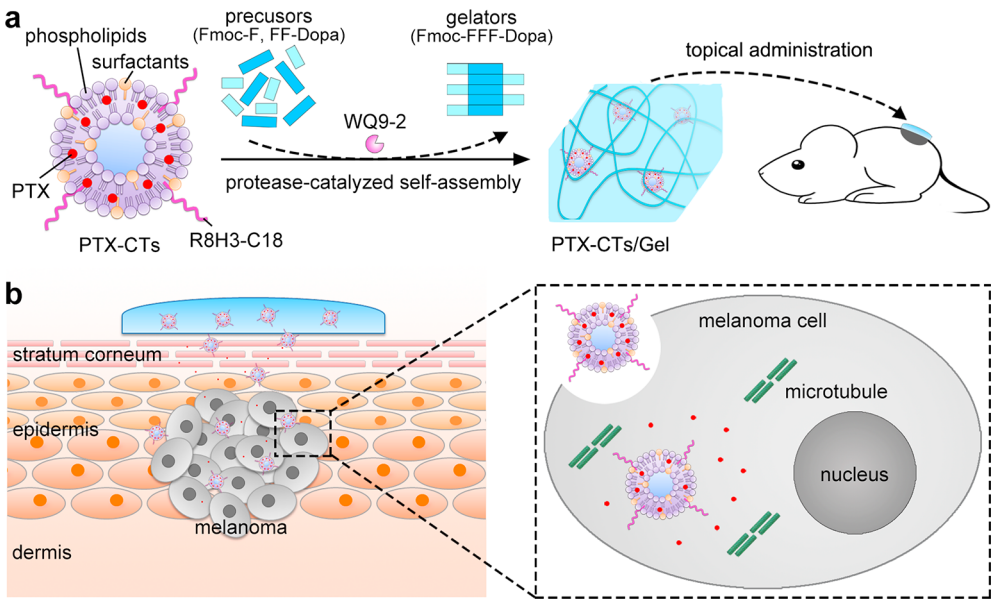

Figure 1. (a) Schematic illustration of preparation and application of PTX-CTs/Gel as a paintable patch for topical drug delivery. (b) Schematic illustration of enhancement on the transdermal efficiency of PTX by the PTX-CTs/Gel for noninvasive chemotherapy of melanoma.

transfersomes own a similar bilayered structure, which can encapsulate both hydrophilic and hydrophobic molecules. Different from liposomes, the transfersomes are more deformable to efficiently penetrate through the small channels in the skin.[25] An inverse relationship between the size and the skin penetration capacity is also present in the transfersome-based transdermal drug delivery. The transfersomes with a size of 120 nm have been reported to exhibit statistically enhanced penetration into the skin compared with the larger ones.[26] In addition, the surfactants incorporated in the transfersomes serve as permeation enhancers to facilitate the transdermal penetration of the transfersomes by increasing stratum corneum lipid fluidity.[27]

Melanoma originated from the melanocytes and typically occurring in the bottom layer of the epidermis is the most dangerous type of skin cancer due to high metastasis and lethality.[28] In addition to surgical resection, clinical treatment options include conventional chemotherapy and radiotherapy as well as emerging biologic therapy and immunotherapy.[29] Either way, transdermal administration provides a promising optional regimen to treat melanoma with maximized therapeutic efficacy and minimized adverse effects.[30−32] However, the challenges still remain on transdermal drug delivery for treatment of melanoma by efficiently overcoming the physiological barriers, including the cutaneous, tumor microenvironmental, and cellular barriers.[33−35]

In this work, we developed a paintable transfersome-embedded oligopeptide hydrogel to enhance transdermal delivery of chemotherapeutic drugs for noninvasive topical chemotherapy of melanoma (Figure 1). Transfersomes are formulated by phospholipids and surfactants including Tween 80 and sodium deoxycholate (Figure 1a). The surfactants play an important role in altering the arrangement and boosting the fluidity of the lipid molecules in the stratum corneum for permeation enhancement.[36] A cell-penetrating peptide (CPP), R8H3, is modified on the transfersomes to further improve both skin and tumor penetration capability of the transfersomes.[37,38] Paclitaxel (PTX) applied for melanoma chemotherapy[39] as a model drug is encapsulated in the CPP-modified transfersomes (CTs). To increase the skin retention property of the PTX-loaded CTs (PTX-CTs), an oligopeptide hydrogel is employed as a reservoir to entrap the PTX-CTs, which is protease (WQ9-2)-catalyzed self-assembled by an oligopeptide, Fmoc-Phe-Phe-Phe-Dopa (Fmoc-FFF-Dopa) formed by precursors, Fmoc-Phe (Fmoc-F) and Phe-Phe-Dopa (FF-Dopa).[40,41]

The PTX-CTs-embedded hydrogel (PTX-CTs/Gel) can be painted as a patch on the skin above the melanoma with prolonged retention time in comparison with the PTX-CT solution (Figure 1b). The PTX-CTs are able to efficiently extrude through the gaps in the stratum coreum into the epidermis where the melanoma cells are located by virtue of a combination of favorable deformability of the transfersomes and the membrane penetration enhancement by the R8H3 peptide. After reaching the melanoma tumor, the PTX-CTs with the help of the R8H3 peptide can penetrate into the deep region of the tumor, be internalized by the tumor cells, and escape from the endosomes.[38] The released PTX from the CTs within the cytoplasm inhibits the proliferation of the melanoma cells by stabilizing the microtubules and preventing their disassembly.[42]

RESULTS AND DISCUSSION

Preparation and Characterization of PTX-CTs. The PTX-Ts consisting of phospholipid, Tween 80, and sodium deoxycholate were prepared using the thin-film dispersion method, which had a hydrodynamic diameter of 71 nm determined by the dynamic laser scattering (Figure 2a). A higher negative charge (−39 mV) of the PTX-Ts was determined compared with that of the PTX-loaded conventional liposomes (PTX-Ls) composed of phospholipid and cholesterol, which results from incorporation of sodium deoxycholate, an anionic surfactant. Stearylated R8H3 composed of a cationic peptide segment containing octaarginine and trihistidine and a stearyl chain was modified on the surface of the PTX-Ts via hydrophobic and electrostatic

DOI: 10.1021/acsnano.8b03800
ACS Nano XXXX, XXX, XXX−XXX

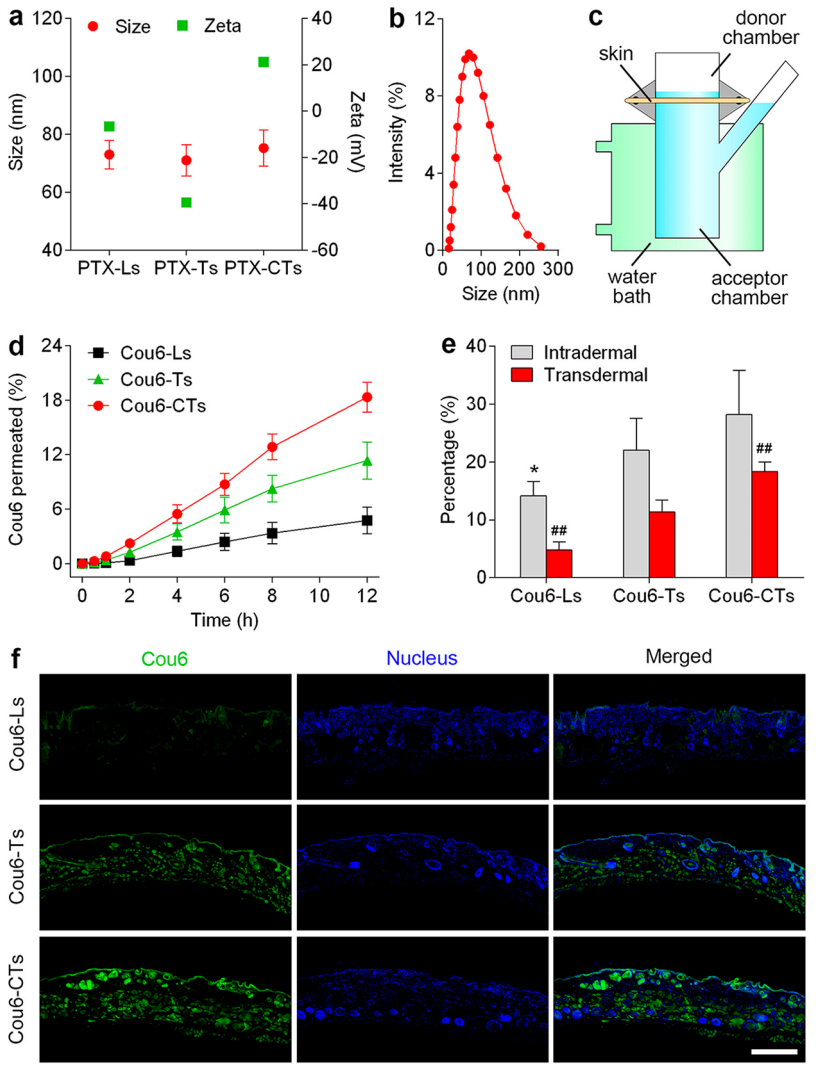

Figure 2. (a) Particle size and zeta potential of different PTX formulations. (b) Size distribution curve of PTX-CTs. (c) Schematic illustration of the Franz diffusion cell system used for the skin permeation study. (d) Cumulative percentage of the Cou6 permeated across the skin from the nude mice after incubation with different Cou6 formulations over time. (e) Cumulative percentage of the intradermal and transdermal Cou6 after the skin was incubated with different Cou6 formulations for 12 h. *$P < 0.05$, compared with Cou6-Ts (intradermal); ##$P < 0.01$, compared with Cou6-Ts (transdermal). (f) Fluorescent images of the skin after incubation with different Cou6 formulations for 4 h. Scale bar: 500 μm.

interactions to acquire the PTX-CTs, which had hydrodynamic diameters of 75 nm (Figure 2b) and a positive charge of +21 mV. The transmission electron microscope (TEM) image showed the morphology of the PTX-CTs (Figure S1). PTX was efficiently encapsulated in the lipid bilayer membrane of the PTX-CTs. The drug-loading capacity and entrapment efficiency of PTX in the PTX-CTs were about 3.2% and 99%, respectively.

The Franz diffusion cell system was employed to evaluate the permeation capability of the CTs through the abdominal skin of the mice (Figure 2c). Coumarin 6 (Cou6), a hydrophobic fluorescent dye, was loaded into the bilayer of the CTs to visualize their transdermal penetration process. The Cou6-loaded formulations were added into the donor chamber, and the amount of the Cou6 molecules permeated across the skin in the medium of the acceptor chamber was determined at different predetermined time intervals. The mean cumulative percentage of the Cou6 permeation through the skin area was about 11.4% in the Cou6-loaded transfersome (Cou6-T) group within 12 h, which was significantly higher than 4.8% of the Cou6-loaded liposome (Cou6-L) group (Figure 2d). The Cou6-Ts showed higher penetration ability through the skin from the nude mice than the Cou6-Ls, which is attributed to the penetration enhancing effect of the surfactants[36] and the highly flexible property of the transfersome.[25] The surfactants of the transfersomes penetrated among the kerotinocytes can change the crystal arrangement and increase the fluidity of the lipid molecules in the stratum corneum, therefore enhancing the permeation of the transfersome. Furthermore, the higher deformability of the transfersomes than that of the liposomes renders them able to squeeze across the small channels in the skin. Significantly, the Cou6-loaded CTs (Cou6-CTs) displayed more favorable skin-penetrating capacity compared with both Cou6-Ls and Cou6-Ts, which had a mean cumulative permeation percentage of 18.3%. Combined with the merit of the transfersome, the R8H3 peptide modified on the Cou6-CTs further facilitates the transdermal penetration. Although the skin penetration

DOI: 10.1021/acsnano.8b03800
ACS Nano XXXX, XXX, XXX−XXX

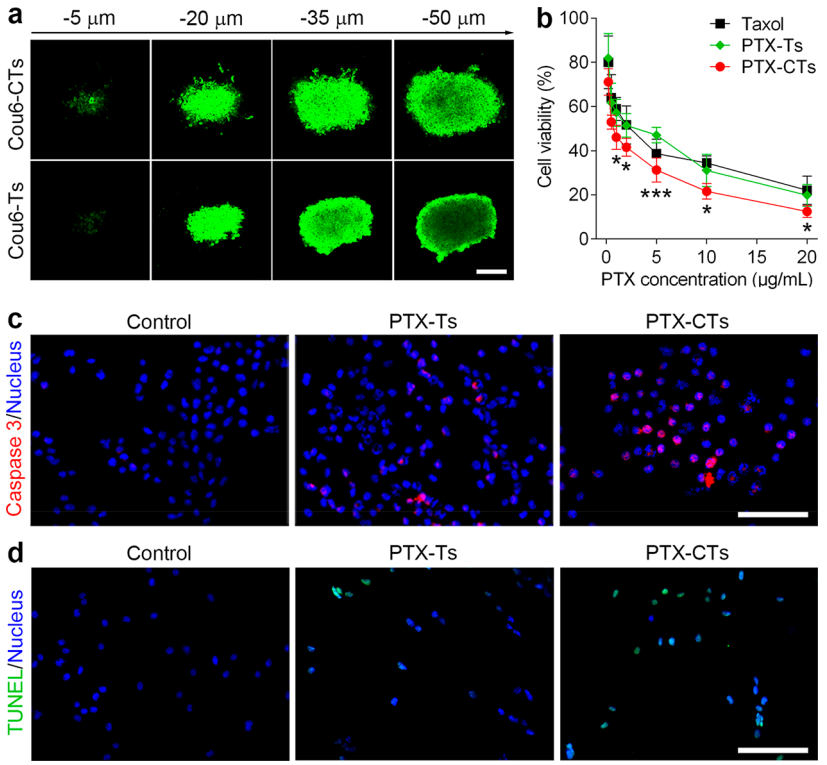

Figure 3. (a) Fluorescent images of the B16F10 melanoma spheroids incubated with the Cou6-CTs and Cou6-Ts for 12 h. The images were obtained using the confocal microscopic tomoscan imaging from the surface to the middle of the tumor spheroid. Scale bar: 100 μm. (b) Viability of the B16F10 melanoma cells incubated with Taxol, PTX-Ts, and PTX-CTs for 24 h. *$P < 0.05$, ***$P < 0.001$, PTX-CTs compared with PTX-Ts. (c, d) Fluorescent images of the B16F10 melanoma cells stained by the caspase 3 activity kit (c) and the TUNEL assay kit (d) after incubation with the PTX-Ts and PTX-CTs for 12 h. Scale bars: 100 μm

mechanism of CPPs, including the R8H3 peptide, still remains debatable, it is speculated to be associated with the transcellular and paracellular pathways. For transcytosis, the R8H3 peptide rich in arginines with guanidine groups shows strong binding on the anionic cell membrane, which facilitates the internalization of nanoparticles. Additionally, histidine containing the imidazole group can improve the intracellular delivery by its proton sponge effect on endosomal escape of nanoparticles. For paracellular pathways, the interaction between the R8H3 peptide and the skin extracellular lipid matrices results in the disruption of the ordered lipid orientation, which generates channels for transporting nanoparticles through the skin. After 12 h of treatment, the skin was harvested, and the intradermal amount of Cou6 was quantified (Figure 2e). The mean cumulative percentage of the Cou6 deposition in the skin was about 28.2% in the Cou6-CT group, higher than 14.2% of the Cou6-L group and 22.0% of the Cou6-T group, which indicates that the CTs present more infiltrating into the skin, thereby yielding increased transdermal permeation. The qualitative results by the confocal microscopic observation were in agreement with the quantitative data (Figure 2f). The fluorescent images showed that higher fluorescent signal of Cou6 was evenly distributed in the skin after 4 h of incubation with the Cou6-CTs, compared with those incubated with either Cou6-Ls or Cou6-Ts. Moreover, the Cou6 signal of the Cou6-CTs was observable in both epidermis and dermis of note, which suggests that the CTs can efficiently penetrate into the deep layers of the skin. In addition, the results of the *in vitro* permeation study performed on the skin with the hair removed from the normal mice further confirmed the enhanced skin permeation efficiency of the CTs (Figure S2).

We further investigated the integrity of the CTs during the skin penetration process. The dual-fluorescence-labeled CTs (Cou6/Rho-CTs) were prepared in which the Cou6 was encapsulated in the bilayer of the CTs, and rhodamine-labeled 1,2-dipalmitoylphosphatidylethanolamine (Rho-PE) was anchored into the lipid membrane. The Cou6/Rho-CTs were deposited on the surface of skin in the donor chamber for 12 h, followed by fluorescent microscopic observation (Figure S3). The Cou6 fluorescent signals were partially colocalized with the Rho signals, which indicates that a significant part of the CTs were intact during the skin-penetration process. On the other hand, some of the Cou6 signals were dissociated with the Rho signals, which is possibly due to the release of Cou6 from the CTs.

Tumor Penetration and *in Vitro* Anticancer Effect of PTX-CTs. After overcoming the skin barriers, poor penetration in solid tumors has also been one of challenges limiting the antitumor efficacy of nanomedicine.[34] To assess the tumor penetration ability of the CTs, a three-dimensional tumor spheroid model mimicking the *in vivo* solid tumor, was used to monitor the tumor permeability of the Cou6-CTs. The established tumor spheroid composed of the murine melanoma (B16F10) cells with the radius of 150 μm was incubated with the Cou6-CTs and Cou6-Ts for 12 h, respectively, followed by the confocal microscopic tomoscan imaging from the surface to the middle of the tumor spheroid (Figure 3a). After the tumor spheroid was treated with the Cou6-CTs, a bright Cou6 fluorescent signal was visualized spreading in the majority of the spherical region. Compara-

DOI: 10.1021/acsnano.8b03800
ACS Nano XXXX, XXX, XXX−XXX

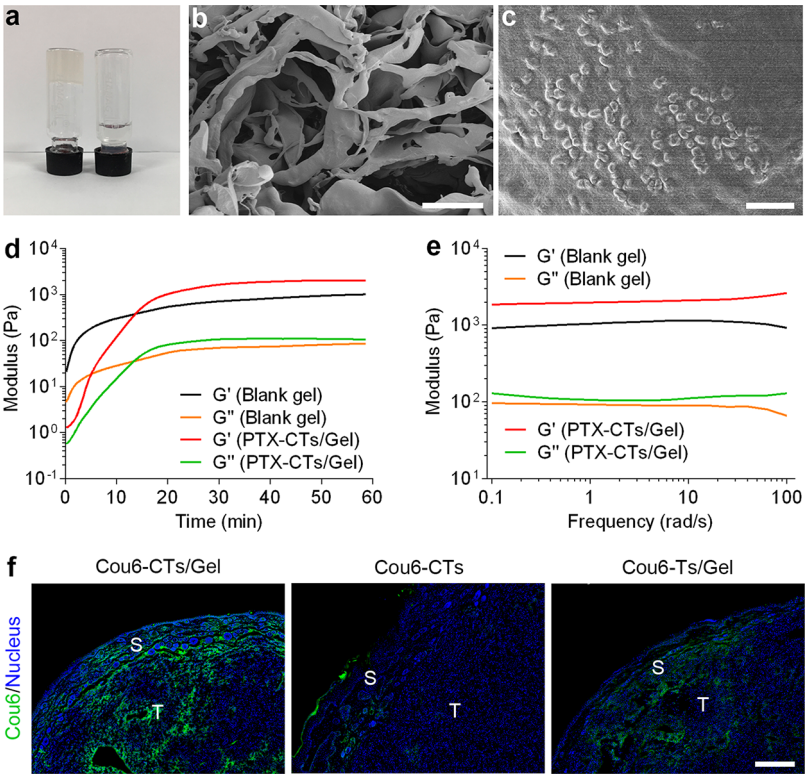

Figure 4. (a) Image of the gelation of the PTX-CTs/Gel. Left: solution containing precursors and PTX-CTs after WQ9-2 was added. Right: solution containing precursors and PTX-CTs. (b, c) SEM images of the PTX-CTs/Gel at low (b) and high (c) magnification. Scale bars: 100 μm (b) and 1 μm (c). (d) Variation in the moduli of the blank hydrogel and PTX-CTs/Gel after WQ9-2 was added over time. (e) Variation in the moduli of the blank hydrogel and PTX-CTs/Gel with the frequency ranging from 0.1 to 100 Hz. (f) Fluorescent images of the tissue section containing the skin layer with the subcutaneous B16F10 melanoma tumor treated with the Cou6-CTs/Gel, Cou6-CT solution, and Cou6-Ts/Gel. The Cou6-CTs/Gel, Cou6-CT solution, and Cou6-Ts/Gel were painted on the skin above the melanoma tumor of the mice once a day. After 3 days, the skin layer with the subcutaneous tumor was harvested to prepare the frozen tissue section. S: skin layer; T: tumor region. Scale bar: 400 μm.

tively, the Cou6-Ts exhibited a weaker tumor penetration capacity than the Cou6-CTs. At the depth of 50 μm from the surface of the tumor spheroid, the Cou6 fluorescent signal was detected to be distributed only at the edge after the tumor spheroid incubated with the Cou6-Ts for 12 h (Figure S4). These data suggest that the R8H3 peptide has a great contribution to the enhancement on the tumor penetration of the transfersomes. Furthermore, the R8H3 peptide modification can also promote the cell membrane permeation of the nanocarriers, which results in increased cellular uptake of the transfersome. The intracellular accumulation of the Cou6-CTs in the B16F10 cells was significantly higher than that of the Cou6-Ts (Figure S5).

The *in vitro* cytotoxicity and the apoptosis-inducing effect of the PTX-CTs toward the B16F10 cells were further investigated. The PTX-CTs displayed higher cytotoxic effect on the B16F10 cells compared with other PTX formulations (Figure 3b). The half-maximal inhibitory concentration of the PTX-CTs against the B16F10 cells was about 0.85 μg/mL, which was lower than 2.12 μg/mL of Taxol and 2.15 μg/mL of the PTX-Ts. The cells treated with the blank CTs without PTX did not show any cell death (Figure S6), which suggests that the cytotoxic effect of the PTX-CTs to the melanoma cells is mainly ascribed to the anticancer activity of PTX rather than the toxicity of the nanocarrier. The data indicate that the PTX-CTs elevate the intracellular concentration of PTX, leading to higher cytotoxicity against the cancer cells. To further evaluate the effect of the PTX-CTs on inducing the cell apoptosis, the activation of the caspase 3, an essential executor of apoptosis in the cells, was monitored using the confocal microscope after the B16F10 cells were treated with the PTX-CTs for 12 h and stained using a caspase 3 activity kit.[43] The red fluorescent signal of the activated caspase 3 within the B16F10 cells after the PTX-CTs treatment was observed to be higher than that treated with the PTX-Ts (Figure 3c), which suggests that treatment with the PTX-CTs leads to an efficient activation of intracellular caspase 3 in the melanoma cells for the induction of apoptosis. The B16F10 cells treated with the PTX-CTs displayed much more massive DNA fragments as shown in green fluorescent signals in the nuclei stained by the terminal deoxynucleotidyl transferase dUTP nick end labeling (TUNEL) assay kit[44] (Figure 3d), which further confirms that the cell death caused by the PTX-CTs is highly associated with the activation of the caspase 3-induced apoptosis of the melanoma cells.

Preparation and Characterization of PTX-CTs/Gel. To realize the paintability and increase the retention of the PTX-CTs on the skin, an enzyme-assisted self-assembled oligopeptide hydrogel was applied as a reservoir for the PTX-CT loading. A protease WQ9-2[41] screened in our laboratory with the optimal catalysis activity was used to trigger the bond formation between the precursors of Fmoc-F and FF-Dopa to acquire the gelator, Fmoc-FFF-Dopa (Figure S7a),[40] which can further self-assemble into the oligopeptide nanofiber-based

DOI: 10.1021/acsnano.8b03800
ACS Nano XXXX, XXX, XXX−XXX

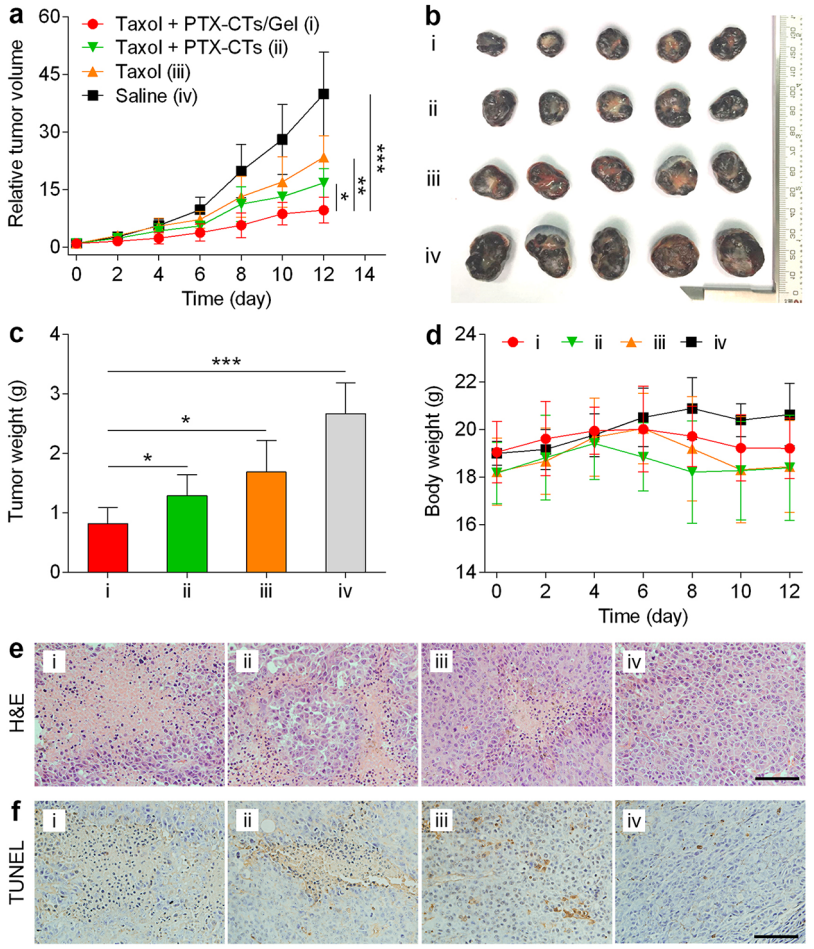

Figure 5. (a) Variation in the relative tumor volume of the B16F10 melanoma-bearing mice treated with different PTX formulations. *P < 0.05, **P < 0.01, ***P < 0.001. (b, c) Tumor image (b) and tumor volume (c) of the mice at day 12 after treatment. *P < 0.05, ***P < 0.001. (d) Variation in the body weight of the mice after treatment. (e, f) Images of the H&E- (e) and TUNEL-stained (f) tumor sections at day 12 after treatment. Scale bars: 100 μm.

hydrogel, as characterized by TEM (Figure S7b). PTX-CTs/Gel with a self-supporting capacity was formed by adding WQ9-2 into the solution containing the PTX-CTs and the precursors (Figure 4a). The microscale structure of the PTX-CTs/Gel was examined by scanning electron microscopy (SEM). The interwoven network formed by the fiber bundles underpinned the hydrogel structure (Figure 4b). A number of the PTX-CTs were visible in the hydrogel as shown in the highly magnified SEM image (Figure 4c).

To analyze the gelation kinetics and viscoelastic properties of the oligopeptide hydrogel, the time and frequency scanning of rheology experiments were carried out. After the addition of WQ9-2 into the precursor solution without the PTX-CTs, both G' (storage modulus) and G'' (loss modulus) values significantly increased with time (Figure 4d). The G' value reached 1000 Pa, up to an order of magnitude higher than the G'' value, which is indicative of a strong mechanical force of the formed hydrogel. The addition of the PTX-CTs slightly slowed the process of gelation but improved the elasticity of nanofibers with the G' value reaching a plateau at about 2000 Pa. The modulus variation of the PTX-CTs/Gel was further investigated with the frequency ranging from 0.1 to 100 Hz (Figure 4e). The modulus of the PTX-CTs/Gel showed a frequency independence at the studied frequency range, which showed that the PTX-CTs/Gel maintains a high elasticity. The Cou6-CTs/Gel showed a consistent skin permeability curve with the Cou6-CT solution but relatively slower transdermal rate obtained using the Franz diffusion cell system (Figure S8), which is attributed to the release of CTs from the hydrogel prior to the skin penetration.

Next, to demonstrate the ability of the oligopeptide hydrogel to improve the skin-penetrating capability of the CTs by prolonging the retention on the skin, the microdistribution of the Cou6-CTs in the skin tissue was explored after the B16F10 melanoma-bearing mice were treated with the Cou6-CTs/Gel. The Cou6-CTs/Gel was plastered on the subcutaneous melanoma tumor of the mice once a day. After 3 days of treatment, the mice were euthanized. The skin layer together with the subcutaneous tumor were sampled, and the tissue section was prepared by the cryotomy, which was subsequently examined by the confocal microscope (Figure 4f). A high intensity of the Cou6 signal was visible to spread in both the skin layer and the tumor region after treatment with the Cou6-CTs/Gel, while the Cou6-CT solution without the support of the hydrogel could not achieve desirable transdermal efficiency *in vivo*. In addition, the Cou6-CTs/Gel allowed deeper skin and tumor penetration than the Cou6-Ts/Gel by virtue of the R8H3 peptide modification. These remarkable differences validates that the oligopeptide hydrogel endues the CTs with

DOI: 10.1021/acsnano.8b03800
ACS Nano XXXX, XXX, XXX−XXX

enhanced retention property, and the CTs promote *in vivo* skin and tumor penetration.

***In Vivo* Anticancer Effect of PTX-CTs/Gel.** The *in vivo* anticancer efficacy of the PTX-CTs/Gel was studied on the B16F10 melanoma-bearing mice in combination with the commercial paclitaxel formulation, Taxol, which is used for chemotherapy of melanoma.[39] The mice were treated by intravenous administration of Taxol every other day accompanied by plastering the tumor with the PTX-CTs/Gel once a day. Treatment with four injections of Taxol inhibited the growth of melanoma. Significantly, the anticancer effect of Taxol was enhanced when combined with the auxiliary treatment with the PTX-CTs/Gel (Figure 5a). Of note, combinatorial treatment of Taxol with the PTX-CTs/Gel showed preferable tumor inhibition effects compared with that of Taxol with the PTX-CT solution, which is due to a combination of the enhanced retention of the PTX-CTs on the skin by the PTX-CTs/Gel and the increased penetration of PTX into the melanoma across the skin by the PTX-CTs. Moreover, the PTX-CTs/Gel also showed greater tumor-inhibiting effects than the PTX-T/Gel in combination with Taxol chemotherapy (Figure S9). This is because of a combination of the enhanced retention of the PTX-CTs on the skin by the PTX-CTs/Gel and the increased penetration of PTX into the melanoma across the skin by the PTX-CTs. The smallest tumor size and the lowest tumor weight of the melanoma harvested from the mice after treatment in the combinational group of Taxol and the PTX-CTs/Gel was found compared with other treatment groups (Figure 5b,c). During this combination treatment, there was no significant change in the body weight of the mice compared with those in the saline group (Figure 5d). A noticeable decrease of the melanoma cells was examined in the tumor tissues of the mice cotreated with Taxol and the PTX-CTs/Gel using hematoxylin and eosin (H&E) staining (Figure 5e and Figure S10). The combination treatment with Taxol and the PTX-CTs/Gel induced the highest level of tumor cell apoptosis in the tumor tissues (Figure 5f). There were no remarkable pathological changes in the normal organs after treatment (Figure S11). In addition, the skin of the nude mice plastered with the CT/Gel once a day for 8 days was harvested for histological analysis (Figure S12). The treatment with the CT/Gel did not induce obvious pathological changes in the skin tissue. We further evaluated the variation in the activities of alanine transaminase, aspartate transaminase, alkaline phosphatase (indicators of liver function), and blood urea nitrogen (indicator of kidney function) in the plasma of the mice after topical treatment with the PTX-CTs/Gel. No marked changes in the indicators were observed compared with those treated with saline (Figure S13), which indicates that the PTX-CTs/Gel formulation provides a safe and efficient strategy for transdermal drug delivery within the studied period.

CONCLUSIONS

In summary, we have developed PTX-CTs/Gel as a paintable patch to enhance the skin and tumor penetration for topical treatment of cutaneous melanoma. The PTX-CTs/Gel was confirmed to improve the retention of the PTX-CTs on the skin. The deformable PTX-CTs presented favorable transdermal efficiency by the aid of the surfactant components and the CPP modification, which also exhibited superior capacity of tumor penetration and intracellular delivery. We showed that the topical chemotherapy using PTX-CTs/Gel combined with the systemic chemotherapy using Taxol suppressed the growth of the melanoma *in vivo*. This topical drug delivery system can be extended for treatment of other skin disorders and diseases.

EXPERIMENTAL SECTION

Preparation and Characterization of PTX-CTs. Transfersomes were prepared through a thin film dispersion method followed by membrane extrusion. Components of soybean phospholipid, Tween 80, and sodium deoxycholate (8:1:1, w:w:w) were dissolved in the mixed organic solvent of chloroform and methanol (2:1, v:v). PTX (3.3% of the total carrier weight) was added in the components for preparation of the PTX-Ts. For preparation of fluorescent-labeled transfersomes, Cou6 (0.02% of the total carrier weight) was added. A thin film was formed after removal of solvent under vacuum using a rotary evaporator at 40 °C for 20 min. After an overnight of vacuum-dry to remove trace organic solvent, the thin film was then hydrated in the deionized water and dispersed by a probe sonicator in an ice–water bath. The PTX-Ts were obtained by extrusion through the membrane with the pore size of 220 nm. The PTX-Ls were prepared by the same method, except that the formulation was composed of phospholipid and cholesterol (4:1, w:/w). Subsequently, the PTX-Ts after precooling were incubated with R8H3-C18 (2.5 mol % of the total lipid weight) at 4 °C for 0.5 h to acquire the final formulation, PTX-CTs.

The entrapment efficiency (EE = $W/W_0 \times 100$) was calculated, where W is the quantity of PTX in the transfersomes after separation by a Sephadex G-50 column and W_0 is the total quantity of PTX in the transfersome solution before separation. For quantitative determination of PTX, the HPLC system (Shimadzu) was applied, which is composed of a degassing unit (DGU-20A_{3R}), a pump (LC-20AD), an auto sampler (SIL-20AC), and a diode-array detector (SPD-M20A). To separate the analytes, an ODS-SP column (Inertsil, 5 μm × 4.6 mm × 250 mm) was used, and the mobile phase was a mixture of methanol and water (70:30, v/v). The detection wavelength was 227 nm. The particle size and zeta potential were analyzed using a zetasizer (Malvern Nano ZS90). The morphology of PTX-CTs was visualized by the TEM (Hitachi HT7700).

Skin Penetration. The transdermal capability of the CTs was investigated using the Franz diffusion cell system. The excised abdominal skin from the nude mice and the normal mice was mounted between donor and acceptor chambers of the system with the stratum corneam facing the donor chamber. A 300 μL portion of various Cou6 formulations at the Cou6 concentration of 5 μg/mL was deposited on the surface of skin in the donor chamber. The acceptor chamber was filled with the mixture medium of phosphate-buffered saline (PBS) and ethanol (3:1, v:v) and kept stirring constantly at 37 °C in a thermostatic water bath. For qualification assay, the mounted skin was collected after 4 h of treatment, washed with PBS repeatedly, polymerized in 4% paraformaldehyde, stained with DAPI, and imaged by a fluorescent microscope (Nikon Eclipse Ci). For quantification assay, 800 μL of medium was sampled from the acceptor chamber at predetermined time points and replaced with an equal volume of fresh medium. The fluorescent intensity of Cou6 in the sampled medium ($\lambda_{ex}/\lambda_{em}$ = 466/504 nm) was measured by a microplate reader (Tecan M1000 Pro). The cumulative percentage of the Cou6 permeated across the skin (Q_n) was calculated according to the following equation

$$Q_n\,(\%) = \frac{VCn + \sum_{i=1}^{n-1} C_i V_i}{A} \times 100$$

where Q_n is the cumulative percentage of the Cou6 permeated across the skin, V the volume of the medium in the acceptor chamber (8 mL), V_i the volume of the medium sampled at different time points (0.8 mL), Cn the concentration of the Cou6 in the medium in the acceptor chamber at different time points, Ci the concentration of the Cou6 in the medium in the acceptor chamber at the ith $(n-1)$ time point, and A the feeding quantity of the Cou6.

DOI: 10.1021/acsnano.8b03800
ACS Nano XXXX, XXX, XXX–XXX

At 12 h, the mounted skin was collected carefully to determine the quantity of Cou6 in the skin. The skin was washed by the hydro-alcoholic solution (50%, v/v) repeatedly to remove the residual Cou6 adhered to the skin. The skin was then cut into small pieces and homogenized in the hydro-alcoholic solution, followed by 1 h of sonication. After centrifugation for 30 min at 5000 rpm, the fluorescent intensity of Cou6 in the supernatant was measured.

To evaluate whether the CTs were intact during the skin penetration, we prepared dual-fluorescence-labeled CTs (Cou6/Rho-CTs) by encapsulating Cou6 and modifying with Rho-PE. The Cou6/Rho-CTs were deposited on the surface of skin in the donor chamber. After 12 h, the skin was collected, washed with PBS repeatedly, polymerized in 4% paraformaldehyde, stained with DAPI, and imaged by the fluorescent microscope.

Preparation and Characterization of PTX-CTs/Gel. The PTX-CTs/Gel was prepared as follows. A 250 μL portion of the homogeneous PTX-CTs (1 mg/mL PTX) suspension was mixed with 550 μL of PBS (pH 7.4) containing Fmoc-F and FF-Dopa followed by addition of 200 μL of the WQ9-2 solution to initiate the gelation. After 4 h of incubation at 37 °C, the PTX-CTs/Gel was obtained. The final concentrations of Fmoc-F and FF-Dopa were 10 and 20 mM, respectively. The morphology was characterized using the TEM and SEM (Hitachi S3400N), respectively.

The solution containing Fmoc-F, FF-Dopa, and the PTX-CTs was deposited on the parallel plate, and the moduli were measured (strain: 2%, frequency: 2 Hz) over time after the WQ9-2 was added. On the other hand, after standing for 4 h, the moduli of the PTX-CTs/Gel were measured at the frequency range from 0.1 to 100 Hz (strain: 2%).

***In Vivo* Skin and Tumor Penetration.** A 0.1 mL portion of the Cou6-CTs/Gel was painted topically on the skin above the tumor once a day for 3 days. Subsequently, the tumor-bearing mice were euthanized, and the skin along with the tumor was harvested. The tissue section was obtained by vertically cutting from the skin to the middle of the tumor, followed by the nucleus counterstaining with DAPI. The tissue section was visualized by the fluorescent microscope. The Cou6 solution and Cou6-Ts/Gel were taken as control groups.

***In Vivo* Antitumor Effect.** Twenty melanoma tumor-bearing nude mice were randomly divided into four groups (5 mice/group) as the tumor volume (length × width^2/2) reached about 0.1−0.15 cm^3. The mice were treated by the following different regimens: (1) intravenous injection of PBS as control group; (2) intravenous injection of Taxol (5 mg/kg) every other day (4 times); (3) intravenous injection of Taxol (5 mg/kg) every other day (4 times) plus plastering the tumor with the PTX-CT solution (1 mg/kg) once a day (8 times); (4) intravenous injection of Taxol (5 mg/kg) every other day (4 times) plus plastering the tumor with the PTX-CTs/Gel (1 mg/kg) once a day (8 times). The tumor length and width as well as the body weight of mice were measured every other day. The mice were euthanatized 12 days after the first treatment, and the tumors and normal tissue were harvested. The tumor sections were examined by the H&E and TUNEL staining, respectively, while the normal tissue sections were investigated by the H&E staining. The stained tissue sections were visualized by a microscope (Olympus IX51).

ASSOCIATED CONTENT

Supporting Information

The Supporting Information is available free of charge on the ACS Publications website at DOI: 10.1021/acsnano.8b03800.

Materials, additional experimental procedures, and supplementary figures (PDF)

AUTHOR INFORMATION

Corresponding Authors

*E-mail: bingfanghe@njtech.edu.cn.
*E-mail: rmo@cpu.edu.cn.

ORCID

Ran Mo: 0000-0003-4010-8879

Notes

The authors declare no competing financial interest.

ACKNOWLEDGMENTS

This work was supported by the National Natural Science Foundation of China (81503012, 81673381) and the Natural Science Foundation of Jiangsu Province of China (BK20150963, BK20150029). This work was also supported by the Program for Jiangsu Province Innovative Research Talents, and the Program for Jiangsu Province Innovative Research Team to R.M. Additionally, we acknowledge financial support from the the fund sponsored by the Jiangsu Synergetic Innovation Center for Advanced Bio-Manufacture (No. XTC1812). We also acknowledge the Public Platform of State Key Laboratory of Natural Medicines at China Pharmaceutical University for the use of analytical instrumentation facilities.

REFERENCES

(1) Yang, G.; Wang, J.; Wang, Y.; Li, L.; Guo, X.; Zhou, S. An Implantable Active-Targeting Micelle-in-Nanofiber Device for Efficient and Safe Cancer Therapy. *ACS Nano* **2015**, *9*, 1161−1174.
(2) Yang, G.; Li, X.; He, Y.; Ma, J.; Ni, G.; Zhou, S. From Nano to Micro to Macro: Electrospun Hierarchically Structured Polymeric Fibers for Biomedical Applications. *Prog. Polym. Sci.* **2018**, *81*, 80−113.
(3) Goyal, R.; Macri, L. K.; Kaplan, H. M.; Kohn, J. Nanoparticles and Nanofibers for Topical Drug Delivery. *J. Controlled Release* **2016**, *240*, 77−92.
(4) Prausnitz, M. R.; Langer, R. Transdermal Drug Delivery. *Nat. Biotechnol.* **2008**, *26*, 1261−1268.
(5) Schoellhammer, C. M.; Blankschtein, D.; Langer, R. Skin Permeabilization for Transdermal Drug Delivery: Recent Advances and Future Prospects. *Expert Opin. Drug Delivery* **2014**, *11*, 393−407.
(6) Menon, G. K.; Cleary, G. W.; Lane, M. E. The Structure and Function of the Stratum Corneum. *Int. J. Pharm.* **2012**, *435*, 3−9.
(7) Prausnitz, M. R. A Practical Assessment of Transdermal Drug Delivery by Skin Electroporation. *Adv. Drug Delivery Rev.* **1999**, *35*, 61−76.
(8) Wang, Y.; Thakur, R.; Fan, Q.; Michniak, B. Transdermal Iontophoresis: Combination Strategies to Improve Transdermal Iontophoretic Drug Delivery. *Eur. J. Pharm. Biopharm.* **2005**, *60*, 179−191.
(9) Murthy, S. N.; Sammeta, S. M.; Bowers, C. Magnetophoresis for Enhancing Transdermal Drug Delivery: Mechanistic Studies and Patch Design. *J. Controlled Release* **2010**, *148*, 197−203.
(10) Azagury, A.; Khoury, L.; Enden, G.; Kost, J. Ultrasound Mediated Transdermal Drug Delivery. *Adv. Drug Delivery Rev.* **2014**, *72*, 127−143.
(11) Prausnitz, M. R. Microneedles for Transdermal Drug Delivery. *Adv. Drug Delivery Rev.* **2004**, *56*, 581−587.
(12) Ye, Y.; Yu, J.; Wen, D.; Kahkoska, A. R.; Gu, Z. Polymeric Microneedles for Transdermal Protein Delivery. *Adv. Drug Delivery Rev.* **2018**, *127*, 106−118.
(13) Lee, H.; Choi, T. K.; Lee, Y. B.; Cho, H. R.; Ghaffari, R.; Wang, L.; Choi, H. J.; Chung, T. D.; Lu, N. S.; Hyeon, T.; Choi, S. H.; Kim, D. H. A Graphene-Based Electrochemical Device with Thermoresponsive Microneedles for Diabetes Monitoring and Therapy. *Nat. Nanotechnol.* **2016**, *11*, 566−572.
(14) Neubert, R. H. Potentials of New Nanocarriers for Dermal and Transdermal Drug Delivery. *Eur. J. Pharm. Biopharm.* **2011**, *77*, 1−2.
(15) Roberts, M. S.; Mohammed, Y.; Pastore, M. N.; Namjoshi, S.; Yousef, S.; Alinaghi, A.; Haridass, I. N.; Abd, E.; Leite-Silva, V. R.;

DOI: 10.1021/acsnano.8b03800
ACS Nano XXXX, XXX, XXX−XXX

Benson, H. A. E.; Grice, J. E. Topical and Cutaneous Delivery Using Nanosystems. *J. Controlled Release* **2017**, *247*, 86−105.
(16) Seong, J. S.; Yun, M. E.; Park, S. N. Surfactant-Stable and pH-Sensitive Liposomes Coated with N-Succinyl-Chitosan and Chitooligosaccharide for Delivery of Quercetin. *Carbohydr. Polym.* **2018**, *181*, 659−667.
(17) Rai, V. K.; Mishra, N.; Yadav, K. S.; Yadav, N. P. Nanoemulsion as Pharmaceutical Carrier for Dermal and Transdermal Drug Delivery: Formulation Development, Stability Issues, Basic Considerations and Applications. *J. Controlled Release* **2018**, *270*, 203−225.
(18) Yang, Y.; Pearson, R. M.; Lee, O.; Lee, C. W.; Chatterton, R. T.; Khan, S. A.; Hong, S. Dendron-Based Micelles for Topical Delivery of Endoxifen: A Potential Chemo- Preventive Medicine for Breast Cancer. *Adv. Funct. Mater.* **2014**, *24*, 2442−2449.
(19) Lee, H. W.; Lee, J. H.; Kim, J. S.; Mun, J. H.; Chung, J. H.; Koo, H.; Kim, C. H.; Yun, S. H.; Hahn, S. K. Hyaluronate-Gold Nanorod/DR5 Antibody Complex for Noninvasive Theranosis of Skin Cancer. *ACS Appl. Mater. Interfaces* **2016**, *8*, 32202−32210.
(20) Siu, K. S.; Chen, D.; Zheng, X. F.; Zhang, X. S.; Johnston, N.; Liu, Y. L.; Yuan, K.; Koropatnick, J.; Gillies, E. R.; Min, W. P. Non-Covalently Functionalized Single-Walled Carbon Nanotube for Topical siRNA Delivery into Melanoma. *Biomaterials* **2014**, *35*, 3435−3442.
(21) Raju, G.; Katiyar, N.; Vadukumpully, S.; Shankarappa, S. A. Penetration of Gold Nanoparticles Across the Stratum Corneum Layer of Thick-Skin. *J. Dermatol. Sci.* **2018**, *89*, 146−154.
(22) Rancan, F.; Gao, Q.; Graf, C.; Troppens, S.; Hadam, S.; Hackbarth, S.; Kembuan, C.; Blume-Peytavi, U.; Rühl, E.; Lademann, J.; Vogt, A. Skin Penetration and Cellular Uptake of Amorphous Silica Nanoparticles with Variable Size, Surface Functionalization, and Colloidal Stability. *ACS Nano* **2012**, *6*, 6829−6842.
(23) Ashtikar, M.; Nagarsekar, K.; Fahr, A. Transdermal Delivery from Liposomal Formulations - Evolution of the Technology over the Last Three Decades. *J. Controlled Release* **2016**, *242*, 126−140.
(24) Benson, H. A. Transfersomes for Transdermal Drug Delivery. *Expert Opin. Drug Delivery* **2006**, *3*, 727−737.
(25) Elsayed, M. M. A.; Abdallah, O. Y.; Naggar, V. F.; Khalafallah, N. M. Deformable Liposomes and Ethosomes: Mechanism of Enhanced Skin Delivery. *Int. J. Pharm.* **2006**, *322*, 60−66.
(26) Verma, D. D.; Verma, S.; Blume, G.; Fahr, A. Particle Size of Liposomes Influences Dermal Delivery of Substances into Skin. *Int. J. Pharm.* **2003**, *258*, 141−151.
(27) Marwah, H.; Garg, T.; Goyal, A. K.; Rath, G. Permeation Enhancer Strategies in Transdermal Drug Delivery. *Drug Delivery* **2016**, *23*, 564−578.
(28) Miller, A. J.; Mihm, M. C. Mechanisms of Disease - Melanoma. *N. Engl. J. Med.* **2006**, *355*, 51−65.
(29) Rigel, D. S.; Carucci, J. A. Malignant Melanoma: Prevention, Early Detection, and Treatment in the 21st Century. *Ca-Cancer J. Clin.* **2000**, *50*, 215−236.
(30) Wang, C.; Ye, Y.; Hochu, G. M.; Sadeghifar, H.; Gu, Z. Enhanced Cancer Immunotherapy by Microneedle Patch-Assisted Delivery of Anti-PD1 Antibody. *Nano Lett.* **2016**, *16*, 2334−2340.
(31) Ye, Y.; Wang, C.; Zhang, X.; Hu, Q.; Zhang, Y.; Liu, Q.; Wen, D.; Milligan, J.; Bellotti, A.; Huang, L.; Dotti, G.; Gu, Z. A Melanin-Mediated Cancer Immunotherapy Patch. *Sci. Immunol.* **2018**, *2*, No. eaan5692.
(32) Beack, S.; Kong, W. H.; Jung, H. S.; Do, I. H.; Han, S.; Kim, H.; Kim, K. S.; Yun, S. H.; Hahn, S. K. Photodynamic Therapy of Melanoma Skin Cancer Using Carbon Dot - Chlorin e6-Hyaluronate Conjugate. *Acta Biomater.* **2015**, *26*, 295−305.
(33) Alexander, A.; Dwivedi, S.; Ajazuddin; Giri, T. K.; Saraf, S.; Saraf, S.; Tripathi, D. K. Approaches for Breaking the Barriers of Drug Permeation through Transdermal Drug Delivery. *J. Controlled Release* **2012**, *164*, 26−40.
(34) Jain, R. K.; Stylianopoulos, T. Delivering Nanomedicine to Solid Tumors. *Nat. Rev. Clin. Oncol.* **2010**, *7*, 653−664.
(35) Blanco, E.; Shen, H.; Ferrari, M. Principles of Nanoparticle Design for Overcoming Biological Barriers to Drug Delivery. *Nat. Biotechnol.* **2015**, *33*, 941−951.
(36) Namdeo, A.; Jain, N. Liquid Crystalline Pharmacogel Based Enhanced Transdermal Delivery of Propranolol Hydrochloride. *J. Controlled Release* **2002**, *82*, 223−236.
(37) Jiang, T. Y.; Zhang, Z. H.; Zhang, Y. L.; Lv, H. X.; Zhou, J. P.; Li, C. C.; Hou, L. L.; Zhang, Q. Dual-Functional Liposomes Based on pH-Responsive Cell-Penetrating Peptide and Hyaluronic Acid for Tumor-Targeted Anticancer Drug Delivery. *Biomaterials* **2012**, *33*, 9246−9258.
(38) Jiang, T. Y.; Mo, R.; Bellotti, A.; Zhou, J. P.; Gu, Z. Molecule Drugs for Enhanced Therapeutic Efficacy. *Adv. Funct. Mater.* **2014**, *24*, 2295−2304.
(39) Perez, D. G.; Suman, V. J.; Fitch, T. R.; Amatruda, T.; Morton, R. F.; Jilani, S. Z.; Constantinou, C. L.; Egner, J. R.; Kottschade, L. A.; Markovic, S. N. Phase 2 Trial of Carboplatin, Weekly Paclitaxel, and Biweekly Bevacizumab in Patients With Unresectable Stage IV Melanoma A North Central Cancer Treatment Group Study, N047A. *Cancer* **2009**, *115*, 119−127.
(40) Jiang, T.; Shen, S.; Wang, T.; Li, M.; He, B.; Mo, R. A Substrate-Selective Enzyme-Catalysis Assembly Strategy for Oligopeptide Hydrogel-Assisted Combinatorial Protein Delivery. *Nano Lett.* **2017**, *17*, 7447−7454.
(41) Xu, J. X.; Zhou, Z.; Wu, B.; He, B. F. Enzymatic Formation of A Novel Cell-Adhesive Hydrogel Based on Small Peptides with A Laterally Grafted L-3,4-Dihydroxyphenylalanine Group. *Nanoscale* **2014**, *6*, 1277−1280.
(42) Weaver, B. A. How Taxol/Paclitaxel Kills Cancer Cells. *Mol. Biol. Cell* **2014**, *25*, 2677−2681.
(43) Jiang, T. Y.; Sun, W. J.; Zhu, Q. W.; Burns, N. A.; Khan, S. A.; Mo, R.; Gu, Z. Furin-Mediated Sequential Delivery of Anticancer Cytokine and Small-Molecule Drug Shuttled by Graphene. *Adv. Mater.* **2015**, *27*, 1021−1028.
(44) Zhu, Q. W.; Chen, X. J.; Xu, X.; Zhang, Y.; Zhang, C.; Mo, R. Tumor-Specific Self-Degradable Nanogels as Potential Carriers for Systemic Delivery of Anticancer Proteins. *Adv. Funct. Mater.* **2018**, *28*, 1707371.

DOI: 10.1021/acsnano.8b03800
ACS Nano XXXX, XXX, XXX−XXX